Water Adsorption on AnO_2 {111}, {110} and {100} Surfaces (An = U, Pu); A DFT+*U* Study

Bengt E. Tegner*[1], Marco Molinari[2,4], Andrew Kerridge[3], Stephen C. Parker[2], and Nikolas Kaltsoyannis*[1]

[1] School of Chemistry, The University of Manchester,

Oxford Road, Manchester, M13 9PL, UK.

[2]Department of Chemistry, University of Bath,

Claverton Down, Bath, BA2 7AY, UK.

[3] Department of Chemistry, Lancaster University,

Bailrigg, Lancaster, LA1 4YW, UK.

[4]Department of Chemistry, University of Huddersfield,

Queensgate, Huddersfield, HD1 3DH, UK.

*Correspondence: bengt.tegner@manchester.ac.uk, nikolas.kaltsoyannis@manchester.ac.uk

Abstract

The interactions between water and the actinide oxides UO_2 and PuO_2 are important both fundamentally, and when considering the long-term storage of spent nuclear fuel. However, experimental studies in this area are severely limited by plutonium's intense radioactivity, and hence we have recently begun to investigate these interactions computationally. In this article we report the results of plane-wave density functional theory calculations of the interaction of water with the {111}, {110} and {100} surfaces of UO_2 and PuO_2, using a Hubbard-corrected potential (PBE+*U*) approach to account for the strongly-correlated 5f electrons. We find a mix of molecular and dissociative water adsorption to be most stable on the {111} surface, whereas the fully dissociative water adsorption is most stable on the {110} and {100} surfaces, leading to a fully hydroxylated monolayer. From these results we derive water desorption temperatures at various pressures for the different surfaces. These increase in the order {111}<{110}<{100}, and these data are used to propose an alternative interpretation for the two experimentally determined temperature ranges for water desorption from PuO_2.

Introduction

The reprocessing of UO_2-based spent nuclear fuel in the UK has led to the accumulation, over several decades, of significant quantities of highly radioactive PuO_2. Indeed, the UK holds about half the world's civil inventory of PuO_2 (126 tonnes Pu) [1], stored as a powder in stainless steel containers, while the government decides its long term fate. Options include long term storage in a geological disposal facility, or reuse in mixed oxide fuel, but for the time being the material is kept in the steel containers pending a final decision. However, some have buckled, leading to the hypothesis that gas build up has occurred, which might be water vapor due to desorption from the PuO_2, or hydrogen gas from the radiolysis of water, or the reaction of water with PuO_2. It is essential that we fully understand the causes of the container distortions, and hence we are exploring these possibilities computationally as experimental measurements are severely limited. In this contribution, we report our investigations of water adsorption on the low Miller index surfaces of UO_2 and PuO_2, as well as comparing our results with previous work reported in the literature.

Experimental work in this area, especially featuring PuO_2, is very challenging. One of the first mentions of water interactions with PuO_2 was by Haschke *et al*. [2], who suggested that this interaction leads to the formation of the higher oxide PuO_{2+x}. They proposed that water adsorbs in stages, with a first layer of strongly bound, chemisorbed water producing a hydroxylated surface due to dissociation followed by one or more weakly bound layers of molecular water. Earlier, Stakebake [3] measured water desorption temperatures on PuO_2 and reported water desorbing in two distinct temperature ranges, one at 373 – 423 K and another at 573 - 623 K, also suggesting a strongly bound first layer followed by a more weakly bound second layer; he estimated a desorption energy of -2.94 eV for this first layer. Paffet *et al.* [4] confirmed this process and revised the adsorption energy of the first layer to -1.82 eV, and suggested -1.11 eV for the second layer at 371 K.

Previous theoretical investigations have focused mainly on UO_2, and have disagreed as to whether molecular or dissociative adsorption is the more favorable on the {111} surface. Skomurski *et al.* [5] and, more recently, Weck *et al.* [6] found molecular adsorption to be the more favorable on this surface, with adsorption energies of -0.69 eV and -0.77 eV per water molecule respectively, using periodic density functional theory (DFT) with the generalized gradient approximation (GGA) of Perdew and Wang (PW91) used for the exchange-correlation energy. Tian *et al.* [7] also found molecular adsorption to be the stronger on UO_2 {111}, with an adsorption energy of -1.08 eV. These workers employed DFT+*U* [8, 9], a method which addresses the failure of standard DFT functionals to correctly describe the insulating behavior of the actinide dioxides by introducing a Hubbard *U* term to better describe the strongly correlated 5f electrons. By contrast, Bo *et al.* [10], also using DFT+*U*, found that a mixed molecular and dissociative configuration is the most stable on UO_2 {111}, with an adsorption energy of -0.65 eV. These workers also studied water adsorption on the UO_2 {110} and {100} surfaces, finding dissociative adsorption to be the more favorable on both surfaces, with energies of -0.93 and -0.99 eV respectively.

Theoretical studies of water adsorption on PuO_2 are less numerous. Wu *et al.* [11] studied water on the PuO_2 {110} surface using the local density approximation (LDA) and found dissociative adsorption to be favorable with an adsorption energy of -0.49 eV. More recently, Jomard *et al.* [12] also found dissociative adsorption to be the more favorable on the PuO_2 {110} surface with an adsorption energy of -0.95 eV using the PBE+*U* approach. Moreover, Rák *et al.* [13] found that hydroxylation of the AnO_2 {111}, {110} and {100} surfaces stabilizes the wet {110} and {100} surfaces compared with the wet {111}, reversing the trend found for dry surfaces.

We have very recently reported a theoretical study of molecular and dissociative water adsorption on the {111} and {110} surfaces of both UO_2 and PuO_2, using hybrid DFT (PBE0)

within an embedded cluster framework [14]. Adsorption on the {110} surface are stronger than on the {111}. Similar energies are found for molecular and dissociative adsorption on the {111} surfaces, while on the {110} there is a clear preference for dissociative adsorption, as emerges from the periodic DFT studies discussed above, and also in agreement with the experimental suggestions of a fully hydroxylated first layer.

The present paper is organized as follows: we start with a brief description of the DFT+*U* computational methodology used, followed by the results for the dry surfaces. We then discuss water adsorption geometries and energies on the {111}, {110} and {100} surfaces, comparing molecular and dissociative adsorption at various coverages, and finish with predictions of water desorption temperatures over a wide range of pressures. Throughout, we compare our data with previous theoretical and, where possible, experimental results, and propose an alternative explanation for the two distinct temperature ranges seen experimentally for water desorption from PuO_2.

Methodology

All calculations were performed using VASP 5.4.1 [15, 16, 17, 18], a plane-wave DFT code using Projector-Augmented Wave (PAW)-pseudopotentials [16] to describe the ions and employing Monkhorst-Pack (MP) [19, 20] grids for the *k*-space integration. All calculations used a plane wave cut-off of 650 eV and a minimum MP-grid of 5×5×1 *k*-points for the Brillouin zone sampling for the surface simulations and 11×11×11 for the bulk calculations. The generalized gradient approximation of Perdew, Burke, and Ernzerhof (PBE) [21], with a Hubbard *U* correction for the 5f electrons [8, 9], was used for the exchange-correlation energy.

The AnO_2 surfaces are constructed using repeating slabs of 16 AnO_2 units arranged in four layers for the {111} surface and 24 AnO_2 units arranged in six layers for the {110} and {100} surfaces, each with 18 Å of vacuum between each slab. The atom positions are allowed to relax until the net inter-atomic forces are below 0.001 eV/Å. We use **1-k** co-linear magnetic ordering with a net magnetic moment of zero, allowing us to treat the total system as anti-ferromagnetic and thereby reach the correct ground state [23, 24]. We neglect spin-orbit coupling, as earlier results by Rák and co-workers [13] indicate that spin-orbit coupling only has a very small effect on the surface stability.

Surface energies are calculated from

$$E_{surf} = \frac{1}{2\,S}\left(E_{slab}^{N} - N\,E_{bulk}\right)$$

where S is the slab surface area, E_{slab}^{N} is the energy of the slab containing N AnO_2 formula units and E_{bulk} is the bulk reference energy for one AnO_2 formula unit.

The adsorption energy per water molecule is given by the following expression:

$$E_{ads} = \left[E_{(slab+mol)} - \left(E_{slab} + n_{mol} \times E_{mol}\right)\right]/n_{mol}$$

where $E_{(slab+mol)}$ and E_{slab} are the energies of the slab with the adsorbed molecule and the

clean slab, respectively, and E_{mol} is the energy of a water molecule in the gas phase, calculated in VASP using a single water molecule in a large box with a 20 Å side.

Due to the very large number of possible adsorption configurations, we have focused on a small number of likely minimum-energy initial geometries, based on maximizing hydrogen bonding between the adsorbate and the surface at low coverage, and the most stable configuration was kept up to full coverage. Adsorbates are introduced on both sides of the slab to minimize dipole effects, as used by Molinari and co-workers [25]. All figures were drawn using the program VESTA [26].

Dependence on the effective *U* parameter

Previous work has indicated the necessity of using the GGA+*U* formalism [8, 9] to correctly describe the AnO_2 surfaces [13, 27]. To verify the dependence on the effective *U* parameter, U_{eff} = (*U*-*J*), we calculated the adsorption energy of a single water molecule on the {111} surface for U_{eff} ranging from 3 – 5 eV for UO_2 and 4 – 7 eV for PuO_2. We found an energy difference of only 0.05 eV between these extremes, in good agreement with previous work by Weck and colleagues [6], who also found a weak dependence on *U*. In light of this and other studies, using Dudarev's formalism [8] we choose an effective U_{eff} = 4 eV for both UO_2 and PuO_2, as employed previously in the literature.

Results and Discussion

Dry AnO_2 surfaces

Bulk UO_2 and PuO_2 adopt the fluorite structure [28]. We started by constructing our three target low Miller index surfaces by cleaving the bulk along the oxygen-terminated {111}, {110} and {100} planes. The {100} surface was modified by moving half of the oxygens from the bottom to the top, creating a slab without a dipole moment. During relaxation, the An-O bond distances in the outermost layers on the {111}, {110}, and {100} surfaces decrease by about 0.02 Å compared with the bulk.

The calculated surface energies are 0.65, 1.05, and 1.33 J/m^2 for the UO_2 {111}, {110}, and {100} surfaces, and 0.66, 1.13, and 1.59 J/m^2 for the analogous PuO_2 surfaces. This sequence is consistent with other oxide surfaces with fluorite structure, and the calculated surface energies compare well with previous work by Rák *et al.* [13].

Adsorption of water on the AnO_2 {111} surface

A ball-and-stick representation of a single water molecule adsorbing molecularly on the {111} surface supercell is shown in figure 1, and the calculated adsorption energies of molecularly and dissociatively adsorbed water on UO_2 {111} and PuO_2 {111} are collected in table 1. Data from earlier studies on UO_2 from Bo and co-workers [10] as well as Tian and colleagues [7], plus UO_2 and PuO_2 from Rák and colleagues [13], and recent work from our group [14] are shown for comparison. Corresponding data on CeO_2 {111} from Molinari and co-workers [25] are shown in table 2 and selected inter-atomic distances for water on all three metal oxide {111} surfaces are given in table 3.

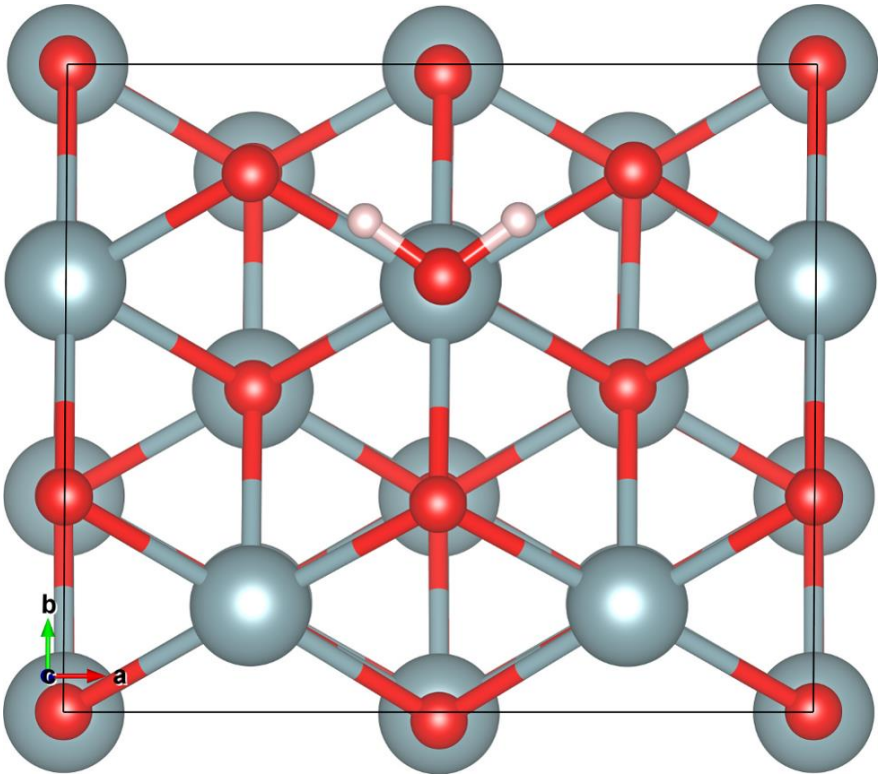

Figure 1: Single water molecule adsorbed molecularly on the 2 × 2 UO_2 {111} surface, yielding a coverage of 25%, i.e. ¼ of a mono-layer. U atoms in gray, oxygen in red and hydrogen in white.

	1 × H_2O	**2 × H_2O**	**3 × H_2O**	**4 × H_2O**
H_2O adsorption	-0.53 *-0.40*	-0.53 *-0.47*	-0.53 *-0.46*	-0.49 *-0.44*
OH + H adsorption	-0.50 *-0.32*	-0.41 *-0.29*	-0.29 *-0.21*	-0.15 *-0.07*
H_2O adsorption [14]	-0.52 *-0.53*	N/A *-0.52*	-0.64 *-0.53*	N/A *-0.59*
OH + H adsorption [14]	-0.63 *-0.45*	-0.56 *-0.39*	-0.53 *-0.42*	N/A *-0.32*
H_2O adsorption [10]	-0.61	N/A	N/A	-0.60
OH + H adsorption [10]	-0.68	N/A	N/A	-0.32
H_2O adsorption [7]	-1.08	N/A	N/A	N/A
OH + H adsorption [7]	-0.68	N/A	N/A	N/A
OH + H adsorption [13]	N/A	N/A	N/A	-0.29 *-0.23*

Table 1: Adsorption energies in eV per water molecule on AnO_2 {111} (An = U, Pu). Data for UO_2 in upright text, PuO_2 data in italics.

	1 × H_2O	**2 × H_2O**	**4 × H_2O**
H_2O adsorption [25]	-0.56	-0.60	-0.57
OH + H adsorption [25]	-0.59	N/A	-0.15

Table 2: Adsorption energies in eV per water molecule on CeO_2 {111}.

	UO_2 {111} + 0.25 – 1.0 ML	**UO_2 {111} + 0.25 – 1.0 ML [10]**	**PuO_2 {111} + 0.25 – 1.0 ML**	**CeO_2 {111} + 0.25 – 1.0 ML [25]**
H_W - O_S	1.96 – 2.28	1.66	2.00 – 2.23	1.99 − 2.13
An_S/Ce_S – H_2O	2.62 – 2.68	2.60 – 2.73	2.62 – 2.68	2.62
An_S/Ce_S - O_WH_W	2.18 – 2.26	2.29 – 2.36	2.20 – 2.26	2.22
An_S/Ce_S - O_SH_W	2.33 – 2.44	N/A	2.30 – 2.43	2.41
O_SH_W - O_WH_W	1.61 – 2.39	N/A	1.56 – 2.29	1.65

Table 3: Selected inter-atomic distances (Å) for molecularly and dissociatively adsorbed water on the UO_2 {111} and PuO_2 {111} surfaces at coverages from 0.25 to 1.0 mono-layers, with results for UO_2 from Bo *et al.* [10] and for CeO_2 from Molinari *et al.* [25]. H_W and O_W denote the hydrogen and oxygen atoms belonging to the water molecule whereas An_S/Ce_S and O_S denote the outermost surface atoms. O_WH_W denotes the hydroxyl molecule made from the dissociated water molecule and O_SH_W denotes the other hydroxyl molecule made from a surface oxygen and the remaining hydrogen.

Examining the adsorption energies for the {111} surface in table 1, we find a slight preference for molecular adsorption at low coverage, increasing with coverage to a marked preference at full coverage, with somewhat lower adsorption energies on PuO_2 compared with UO_2, in good agreement with work by Wellington *et al.* [14]. We interpret this drop in adsorption energy for the dissociative case to weaker hydrogen bonding on the fully hydroxylated surface. We find good agreement between CeO_2 and UO_2/PuO_2 data, particularly at full coverage, strengthening the idea that CeO_2 can be used as a non-radioactive analog of stoichiometric PuO_2 for experimental water adsorption studies [29, 30, 31].

The interatomic distances in table 3 reveal similar hydrogen bond lengths H_W - O_S in UO_2, PuO_2, and CeO_2, suggesting similar bonding. We also find similar actinide -water distances

An_S –H_2O for the three oxides, suggesting similar molecular adsorption geometries. Moreover, the actinide-hydroxyl distances An_S – O_WH_W are shorter than the An_S –H_2O distances, demonstrating that the hydroxyls sit closer to the surface than the molecular water. Furthermore, the hydroxyl-hydroxyl distances O_SH_W - O_WH_W increase with coverage, suggesting weaker intra-molecular hydrogen bonding for the fully dissociative case.

We now discuss mixed adsorption at full coverage, going from fully molecular to fully dissociated. The adsorption energies are shown in table 4. Corresponding data from Bo and colleagues [10] on UO_2 and from Wellington *et al.* [14] are shown for comparison. We again find close similarity between UO_2 and PuO_2, where the 50/50 mixed case gives the strongest adsorption, in good agreement with Bo's work on UO_2 [10] and recent work by Wellington *et al.* [14]. Note, however, that the energy difference between the mixed case and the fully molecular one is only 0.07 eV, and the range of adsorption energies is quite compact. We attribute the increased adsorption energy in the mixed case to the formation of stronger intra-molecular hydrogen bonds on the crowded {111} surface compared with the purely molecular case.

	4 × H_2O	**3 × H_2O + 1 × (OH + H)**	**2 × H_2O + 2 × (OH + H)**	**1 × H_2O + 3 × (OH + H)**	**4 × (OH + H)**
This work	-0.49 *-0.44*	-0.51 *-0.47*	-0.59 *-0.50*	-0.42 *-0.37*	-0.15 *-0.07*
Wellington *et al.* [14]	N/A *-0.59*	-0.71 *-0.55*	-0.74 *-0.65*	-0.68 *-0.55*	N/A *-0.32*
Bo *et al.* [10]	-0.60	-0.60	-0.65	-0.53	-0.32
Rák *et al.* [13]	N/A	N/A	N/A	N/A	-0.29 *-0.23*

Table 4: Adsorption energies in eV per water molecule on AnO_2 {111} (An = U, Pu) for mixed molecular and dissociative adsorption. Data for UO_2 in upright text, PuO_2 data in italics.

Adsorption of water on the AnO_2 {110} surface

The {110} surface is more featured compared with the {111}, with alternating rows of oxygens and actinides which create ridges. The surface actinides have a lower, six-fold coordination compared with the {111} surface, where they are seven-fold coordinated, and with the bulk, where the actinides are eight-fold coordinated. A ball-and-stick representation of a single water molecule adsorbing molecularly on the {110} surface at low coverage is shown in figure 2.

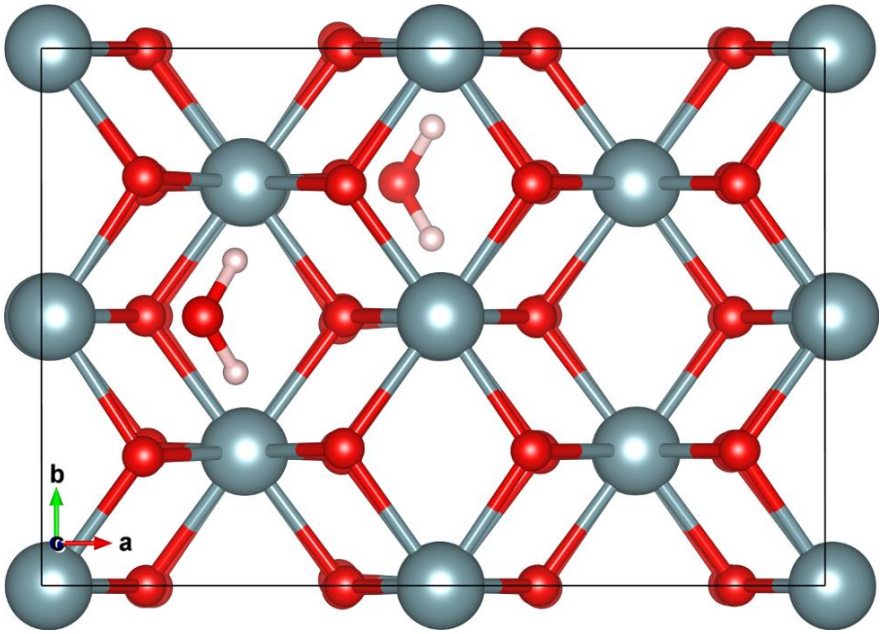

Figure 2: Water adsorbed on the 2 × 2 UO_2 {110} surface, yielding a coverage of 25%, i.e. ¼ of a mono-layer. U atoms in gray, oxygen in red and hydrogen in white. Adsorption occurs on both sides of the slab and, as the two surfaces have equivalent sites that are offset, we can see both the top and the bottom water molecules.

The calculated adsorption energies for molecularly and dissociatively adsorbed water on UO_2 {110} and PuO_2 {110} are collected in table 5. Additional data on UO_2 from Bo and co-workers [10], UO_2 and PuO_2 from Rák and colleagues [13] and recent work by Wellington and others [14], plus PuO_2 data from Jomard and colleagues [12], are again shown for comparison. Corresponding data on CeO_2 {110} from Molinari and co-workers [25] are shown in table 6 while the selected inter-atomic distances are shown in table 7.

	1 × H_2O	**2 × H_2O**	**4 × H_2O**
H_2O adsorption	-0.93 *-0.88*	-0.74 *-0.73*	-0.65 *-0.39*
OH + H adsorption	-1.39 *-1.14*	-1.05 *-0.94*	-1.00 *-0.91*
H_2O adsorption [14]	-1.06 *-0.94*	-0.96 *-1.03*	-0.90 *-0.99*
OH + H adsorption [14]	-1.60 *-1.34*	-1.55 *-1.28*	-1.34 *-1.22*
H_2O adsorption [10]	-0.62	N/A	-0.62 *-0.96*
OH + H adsorption [10]	-1.27	N/A	-0.93
OH + H adsorption [13]	N/A	N/A	-1.05
H_2O adsorption [12]	*-0.87*	*-0.83*	*-0.79*
OH + H adsorption [12]	*-1.12*	*-1.12*	*-0.95*

Table 5: Adsorption energies in eV per water molecule on AnO_2 {110} (An = U, Pu). Data for UO_2 in upright text, PuO_2 data in italics.

	1 × H_2O	**2 × H_2O**	**4 × H_2O**
H_2O adsorption [25]	-0.85	-0.76	N/A
OH + H adsorption [25]	-1.12	-1.00	-0.21

Table 6: Adsorption energies in eV per water molecule on CeO_2 {110}.

	UO_2 {110} + 0.25 – 1.0 ML	**PuO_2 {110} + 0.25 – 1.0 ML**	**CeO_2 {110} + 0.25 – 1.0 ML [25]**
H_W - O_{1S}	2.13 – 2.26	2.14 – 2.21	2.07
An_S/Ce_S – H_2O	2.73	2.72	2.67
An_S/Ce_S - O_WH_W	2.15	2.12	2.14
An_S/Ce_S - O_SH_W	2.44 – 2.58	2.44 – 2.49	2.48 – 2.58
O_SH_W - O_WH_W	3.11	3.05	1.92

Table 7: Selected inter-atomic distances (Å) for molecularly and dissociatively adsorbed water on the UO_2 {110} and PuO_2 {110} surfaces at coverages from 0.25 to 1.0 mono-layers, and results for CeO_2 {110} from Molinari et al. [25]. H_W and O_W denote the hydrogen and oxygen atoms belonging to the water molecule whereas An_S/Ce_S and O_S denote the outermost surface atoms. O_WH_W denotes the hydroxyl molecule made from the dissociated water molecule and O_SH_W denotes the other hydroxyl molecule made from a surface oxygen and the remaining hydrogen.

The adsorption energy data in table 5 reveal good agreement with earlier studies on UO_2 and PuO_2, with the added observation that unlike the {111} surface, there is a clear preference for dissociative adsorption at all coverages on the {110} surface, leading to the prediction that this surface should be fully hydroxylated. This trend is consistent across all previous studies, despite the slightly different equilibrium geometries found. A possible reason for this preference is the lower coordination of the actinide ions at the {110} surface compared with the {111}; the preference for the stronger An–OH bond vs the An–OH_2 will be more pronounced in the less coordinated case. Note that we again find good agreement with ceria at all coverages.

The interatomic distances in table 7 again reveal similar hydrogen bond distances H_W - O_S for UO_2 and PuO_2, suggesting similar hydrogen bonds are present. We also find similar An_S – H_2O distances, suggesting similar adsorption geometries. Moreover, the An_S – O_WH_W distances are again shorter, again demonstrating that the hydroxyls sit closer to the surface than the molecular water. However, despite the O_SH_W - O_WH_W hydroxyl distances being larger than on the {111} surface, we do not see any changes with coverage on the {110} surface that would suggest weaker intra-molecular hydrogen bonding, unlike the {111} surface.

As with {111}, we now investigate mixed adsorption on the {110} surface at full coverage, going from fully molecular to fully hydroxylated. The adsorption energies are shown in table 8. Corresponding data from Bo and colleagues [10], Rák et al. [13], Wellington and others [14], and Jomard and coworkers [12], are shown for comparison. Unlike the {111} surface, we find the fully dissociated case to be the most stable for the {110}, supporting our previous predictions of a fully hydroxylated first layer [14]. Note, however, that Bo and co-workers [10] find a very slight preference for mixed adsorption on UO_2 {110}, which neither we nor Wellington et al.[14], observe.

	4 × H_2O	**3 × H_2O + 1 × (OH + H)**	**2 × H_2O + 2 × (OH + H)**	**1 × H_2O + 3 × (OH + H)**	**4 × (OH + H)**
This work	-0.65 *-0.39*	N/A*	-0.84 *-0.83*	-0.84 *-0.78*	-1.00 *-0.91*
Wellington *et al.* [14]	-0.90 *-0.99*	-1.02 *-1.08*	-1.18 *-1.16*	-1.24 *-1.13*	-1.34 *-1.22*
Bo *et al.* [10]	-0.62	-0.82	-1.00	-0.98	-0.93
Rák *et al.* [13]	N/A	N/A	N/A	N/A	-1.05 *-0.96*
Jomard *et al.* [12]	*-0.79*	*N/A*	*N/A*	*N/A*	*-0.95*

Table 8: Adsorption energies in eV per water molecule on AnO_2 {110} (An = U, Pu) for mixed molecular and dissociative adsorption. Data for UO_2 in upright text, PuO_2 data in italics. * We were unable to converge the correct magnetic state for this configuration.

Adsorption of water on the AnO_2 {100} surface

The {100} surface consists of alternating layers of An and O atoms, where the surface charge depends on the termination. This forces us to move half the oxygen atoms from bottom to the top to balance the charge. We again adsorb on both surfaces to improve symmetry and avoid dipole effects. The surface actinides again have a lower, six-fold coordination compared with the bulk. A ball-and-stick representation of a single water adsorbing on the {100} surface is shown in figure 3.

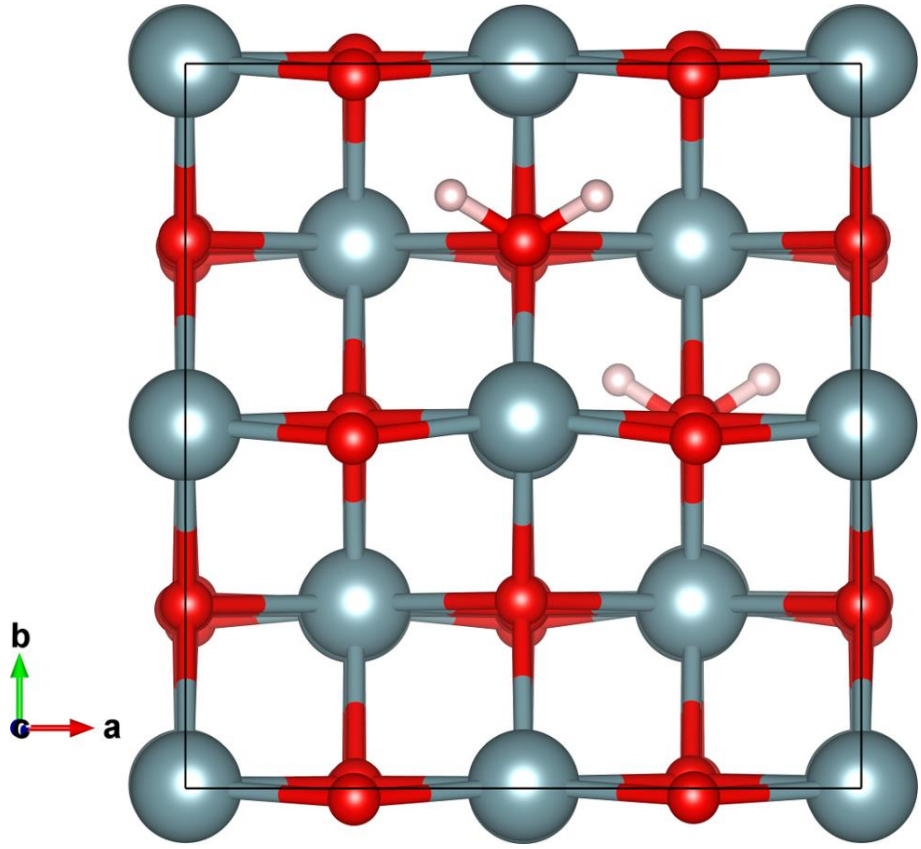

Figure 3: Water adsorbed on the 2 × 2 UO_2 {100} surface, yielding a coverage of 25%, i.e. ¼ of a mono-layer. U atoms in gray, oxygen in red and hydrogen in white. Adsorption occurs on both sides of the slab and, as the two surfaces have equivalent sites that are offset, we can see both the top and the bottom water molecules.

Calculated adsorption energies for molecularly and dissociatively adsorbed water on UO_2 {100} and PuO_2 {100} are given in table 9. Additional data on UO_2 from Bo and co-workers [10], UO_2 and PuO_2 from Rák and colleagues [13] are again shown for comparison. Corresponding data on CeO_2 {100} from Molinari and co-workers [25] are shown in table 10 and selected inter-atomic distances are shown in table 11.

	1 × H_2O	**2 × H_2O**	**4 × H_2O**
H_2O adsorption	-0.97 *-1.12*	-0.87 *-1.00*	-0.86 *-0.95*
OH + H adsorption	-1.55 *-1.76*	-1.44 *-1.64*	-1.01 *-1.37*
H_2O adsorption [10]	-1.02	-0.93	-0.91
OH + H adsorption [10]	-1.71	-1.55	-0.99
OH + H adsorption [13]	N/A	N/A	-1.29 *-1.46*

Table 9: Adsorption energies in eV per water molecule on AnO_2 {100} (An = U, Pu). Data for UO_2 in upright text, PuO_2 data in italics.

	1 × H_2O	**2 × H_2O**	**4 × H_2O**
H_2O adsorption [25]	-1.00	N/A	-0.89
OH + H adsorption [25]	-1.57	-1.73/-0.87	-0.89

Table 10: Adsorption energies in eV per water molecule on CeO_2 {100}.

	UO_2 {100} + 0.25 – 1.0 ML	**PuO_2 {100} + 0.25 – 1.0 ML**	**CeO_2 {100} + 0.25 – 1.0 ML [25]**
H_W - O_{1S}	1.75 – 1.97	1.71 – 1.92	1.97 – 2.11
An_S/Ce_S – H_2O	2.57 – 2.84	2.50 – 2.89	2.64 – 2.70
An_S/Ce_S - O_WH_W	2.26 – 2.35	2.29 – 2.34	2.34 – 2.37
An_S/Ce_S - O_SH_W	2.34 – 2.46	2.36 – 2.51	2.36 – 2.45
O_SH_W - O_WH_W	2.77 – 2.96	2.69 – 2.91	2.52

Table 11: Selected inter-atomic distances (Å) for molecularly and dissociatively adsorbed water on the UO_2 {100} and PuO_2 {100} surfaces at coverages from 0.25 to 1.0 mono-layers, and results for CeO_2 {100} from Molinari et al. [25]. H_W and O_W denote the hydrogen and oxygen atoms belonging to the water molecule whereas An_S/Ce_S and O_S denote the outermost surface atoms. O_WH_W denotes the hydroxyl molecule made from the dissociated water molecule and O_SH_W denotes the other hydroxyl molecule made from a surface oxygen and the remaining hydrogen.

Examining the energies in table 9, we again find a good agreement with earlier studies on UO_2 {100}. As with the {110} surface, there is a clear preference for dissociative adsorption at all coverages on the {100} surface; hence both the {110} and {100} surfaces are predicted

to be fully hydroxylated. This again might be due to the lower An coordination at the {100} surface, where the hydroxyls allow stronger bonding and improved coordination versus molecular water. Moreover, we note that unlike the {111} and {110} surfaces, PuO_2 {100} has larger adsorption energies compared with UO_2 {100}.

Inspecting the inter-atomic distances in table 11, we find shorter hydrogen bond distances H_W - O_S for the AnO_2 {100} surfaces, suggesting stronger bonds compared to the {111} and {110} surfaces. There is also a slight distortion of the surface oxygens, shortening the H_W - O_S bond. We again find similar An_S – H_2O distances for both UO_2 and PuO_2, suggesting the same type of adsorption. Moreover, the An_S – O_WH_W distances are again shorter than the An_S – H_2O distances, again suggesting the hydroxyls sit closer to the surface than the molecular water. However, despite the O_SH_W - O_WH_W hydroxyl distances again being larger than on the {111} surface, like with the {110} surface, we do not see any changes with increasing coverage on the {100} surface that would indicate weaker intra-molecular hydrogen bonding.

As before, we again investigate mixed adsorption at full coverage, going from fully molecular to fully hydroxylated. The adsorption energies are shown in table 12. Corresponding data from Bo *et al.* [10] and Rák and co-workers [13] shown for comparison. For both UO_2 and PuO_2, there is a general trend towards increased favorability for all-dissociative adsorption, although for UO_2 the most stable arrangement is a three-to-one ratio of dissociative to molecular. We attribute this to slightly stronger hydrogen bonding in this particular case, due the presence of a shorter hydrogen bond of 1.62 Å between the adsorbed water molecule and the hydroxyls on the surface. Unlike {111} and {110}, we find larger adsorption energies on PuO_2 {100} than UO_2 {100} for the more dissociative cases.

	4 × H_2O	**3 × H_2O + 1 × (OH + H)**	**2 × H_2O + 2 × (OH + H)**	**1 × H_2O + 3 × (OH + H)**	**4 × (OH + H)**
This work	-0.86 *-0.95*	-0.96 *-0.78*	-0.95 *-1.21*	-1.24 *-1.37*	-1.01 *-1.37*
Bo *et al.* [10]	-0.91	N/A	N/A	N/A	-0.99
Rák *et al.* [13]	N/A	N/A	N/A	N/A	-1.29 *-1.46*

Table 12: Adsorption energies on AnO_2 {100} (An = U, Pu) for mixed molecular and dissociative adsorption. Data for UO_2 in upright text, PuO_2 data in italics.

To summarize the adsorption data for the three target surfaces, we find that on the {111} surface there is a slight preference for a 50/50 mix of molecular and dissociative adsorption for both UO_2 and PuO_2, although the difference in adsorption energy is only 0.06 – 0.1 eV/water molecule compared with the fully molecular case. By contrast, on the {110} and {100} surfaces there is a clear preference for dissociative adsorption for both oxides, leading us to predict that both of these surfaces will be fully hydroxylated. The calculated adsorption energies of -0.91 eV and -1.37 eV for the hydroxylated PuO_2 {110} and {100} surfaces agree reasonably well with the adsorption energies reported by Paffet *et. al.* [4] of -1.11 eV and -1.82 eV; further comparison with experimental data is made in the next section.

Finally, we note that Bo *et. al.* [32] have recently investigated water adsorption on the {111}, {110}, and {100} surfaces of NpO_2. Although this oxide is not the focus of our work, the fact that it has the same crystal structure as UO_2 and PuO_2, and that Np lies between U and Pu in the actinide series, warrants a brief comparison with our data. In general, the conclusions for NpO_2 are the same as the present ones for UO_2 and PuO_2. For both a single water molecule (0.25 ML), and a coverage corresponding to one ML, the energies of both molecular and dissociative adsorption increase in the order {111} < {110} < {100}. Also as in our study, there is a preference for mixed adsorption on {111} and fully dissociate adsorption on {100},

though by contrast to our work, mixed adsorption is preferred over fully dissociative on NpO_2 {110}.

Water desorption temperature (T_d) from AnO_2 surfaces

We have investigated the stability of the monolayer-covered UO_2 and PuO_2 surfaces by calculating the temperature of water desorption (T_d), with the aim of predicting the temperatures at which wet surfaces become dry for a given partial pressure of water. The temperature of desorption at a given pressure is calculated from the equation below, which has been used previously for other material surfaces [25, 33, 34, 35].

$$\gamma_{s,wet,(T,p)} = \gamma_{s,dry} + \left(C \times \left(E_{ads,(T)} - RTln(p/p_0)\right)\right)$$

The surface energy of the dry surface is defined as $\gamma_{s,dry} = \left(E_{slab,dry} - E_{bulk}\right)/2S$ with $E_{slab,dry}$ the energy of the dry slab, E_{bulk} the energy of AnO_2 bulk and $\boldsymbol{S}$ the surface area. The adsorption energy per water molecule is $E_{ads,(T)} = E_{slab,wet} - \left(E_{slab,dry} + n_{H_2O} \times E_{H_2O,(T)}\right)/n_{H_2O}$ with $E_{slab,wet}$ the energy of the monolayer adsorbed slab, n_{H_2O} the number of adsorbed water molecules and $E_{H_2O,(T)} = E_{H_2O,(g)} - TS^o_{(T)}$ where $S^o_{(T)}$ is the experimental entropy of gaseous water in the standard state [36], given by $S^o_{(T)} = 1.4347^{-7}x^3 - 3.2221^{-4}x^2 + 2.8391^{-1}x + 1.2846^{-2}$. C is the coverage in mol/m^2, E_{ads} is the adsorption energy in J/mol, T is the temperature, and p and p^0 are the partial pressures of water chosen and in the standard state (1 bar), respectively.

In Table 13 we give the T_d data for the most stable fully covered configuration for each surface. Desorption temperatures for less stable configurations on each surface can be found in the Supplementary Information, tables S1–S6. Water is predicted to desorb from the AnO_2 {111} surfaces at temperatures between 120 – 319 K, whereas it will remain on the {110} and {100} until temperatures of 208 – 650 K depending on the vapor pressure. We find

slightly lower desorption temperatures for the PuO_2 {111} and {110} surfaces than for UO_2, which is to be expected from the slightly lower adsorption energies. Moreover, we find the highest desorption temperatures for fully hydroxylated PuO_2 {100}, again as expected from the higher adsorption energies found for this system. Our temperatures compare well with earlier work on CeO_2 by Molinari *et al.* [25], who found desorption temperatures of 325 K for the {111} surface, 575 K for the hydroxylated {110} surface and 825 K for the hydroxylated {100} surface, all at atmospheric pressure.

As noted in the introduction, Stakebake's experiments[3] found two distinct temperature ranges for water desorption from PuO_2, 373 – 423 K and 573 - 623 K, the latter being interpreted as being due to waters bound directly to the PuO_2 surface, with the lower range due to more weakly bound second layer (or above) waters. An alternative explanation, on the basis of our calculations, is that these ranges are due to water desorbing from the most strongly bound layers on the {110} and {100} surfaces respectively. Future calculations of multiple layers of water on our target surfaces will give further insight into this suggestion.

Conf. / Pressure	**UO_2 {111} + 2 × H_2O + 2 × (OH + H)**	**PuO_2 {111} + 2 × H_2O + 2 × (OH + H)**	**UO_2 {110} + 4 × (OH + H)**	**PuO_2 {110} + 4 × (OH + H)**	**UO_2 {100} + 1 × H_2O + 3 × (OH + H)**	**PuO_2 {100} + 4 × (OH + H)**
p = 10^{-13} bar	138	120	228	208	271	302
p = 10^{-7} bar	186	162	301	276	356	396
p = 1 bar	300	265	472	434	555	615
p = 3 bar	313	277	490	452	577	638
p = 5 bar	319	282	499	460	587	650

Table 13: Calculated water desorption temperatures in K as a function of pressure for the

most stable fully covered configurations on the {111}, {110} and {100} surfaces of UO_2 and PuO_2.

Conclusions

We have presented a comprehensive study on the water adsorption on the three low Miller index surfaces of UO_2 and PuO_2, comparing molecular and dissociative adsorption at monolayer coverage. This is the first time that data for all three surfaces of both target oxides have been calculated in a single study. We find a mix of molecular and dissociative adsorption to be most stable on the {111} surface, and that fully dissociative adsorption is the most stable configuration on the {110} and {100} surfaces, leading to a fully hydroxylated monolayer.

We have used our calculated adsorption energies to predict desorption temperatures of the most stable configurations for each oxide and surface. Our results suggest that water is present as adsorbed hydroxyl groups on the {110} and {100} surfaces even at elevated temperatures and pressures, conditions likely to be found in the UK's PuO_2 storage canisters. Our data for PuO_2 lead us to tentatively ascribe experimentally determined desorption temperature ranges to desorption from the hydroxylated {110} and {100} surface monolayers.

We are continuing to explore water adsorption on the AnO_2 surfaces, now tackling more complex problems such as defect surfaces and multiple water layers, and will report the results of these studies, and their implications for the PuO_2 storage canisters, in future contributions.

Acknowledgements

We would like to thank the EPSRC's "DISTINCTIVE" consortium (http://www.distictiveconsortium.org, EP/L014041/1) for funding. We also thank the University of Manchester for computing resources via the Computational Shared Facility (CSF) and for access to the "Polaris" cluster at the N8 HPC Centre of Excellence, provided and funded by the N8 consortium and EPSRC (Grant No.EP/K000225/1). The Centre is co-ordinated by the Universities of Leeds and Manchester. We also thank University College London for computing resources *via* Research Computing's "Legion" cluster (Legion@UCL) and associated services, and the "Iridis" facility of the e-Infrastructure South Consortium's Centre for Innovation. We are also grateful to the HEC Materials Chemistry Consortium, which is funded by EPSRC (EP/L000202), for access to ARCHER, the UK's National Supercomputing Service (http://www.archer.ac.uk). Finally, we thank Howard Sims and Robin Orr of the National Nuclear Laboratory, and Jeffrey Hobbs and Helen Steele at Sellafield Ltd, for helpful discussions. All data supporting this study are openly available 482 from the University of Manchester data archive at DOI: 48310.15127/1.306778.

Supporting information

Calculated desorption temperatures from AnO_2 {111}, {110} and {100} surfaces (An = U, Pu) at various pressures (tables S1–S6). Ball and stick representations of the geometries of all the stable adsorption structures. (figures S1–S56).

References

(1) Global Fissile Materials Report 2015. http://fissilematerials.org/library/gfmr15.pdf (accessed Dec 14, 2016).

(2) Haschke, J. M.; Ricketts, T. E. Adsorption of Water on Plutonium Dioxide. *J. Alloys Compd*. **1997**, *252*, 148–156.

(3) Stakebake, J. L.Thermal Desorption Study of the Surface Interactions between Water and Plutonium Dioxide. *J. Phys. Chem*. **1973**, *77*, 581–586.

(4) Paffett, M.; Kelly, D.; Joyce, S.; Morris, J.; Veirs, K. A Critical Examination of the Thermodynamics of Water Adsorption on Actinide Oxide Surfaces. *J. Nucl. Mater*. **2003**, *322*, 45–56.

(5) Skomurski, F . N.; Shuller, L. C.; Ewing, R. C.; Becker, U. Corrosion of UO_2 and ThO_2: A Quantum-Mechanical Investigation. *J. Nucl. Mater*. **2008**, *375*, 290–310.

(6) Weck, P. F.; Kim, E.; Jové-Colón, C. F.; Sassani, D. C. On the Role of Strong Electron Correlations in the Surface Properties and Chemistry of Uranium Dioxide. *Dalton Trans*. **2013**, *42*, 4570–4578.

(7) Tian, X-f.; Wang, H.; Xiao, H-x.; Gao, T. Adsorption of Water on UO_2 (1 1 1) Surface: Density Functional Theory Calculations. *Comput. Mater. Sci*. **2014**, *91*, 364–371.

(8) Dudarev, S. L.; Nguyen Manh, D.; Sutton, A. P. Effect of Mott-Hubbard Correlations on the Electronic Structure and Structural Stability of Uranium Dioxide. *Philos. Mag. Part B* **1997**, *75*, 613–628.

(9) Liechtenstein, A. I.; Anisimov, V. I.; Zaanen, J. Density-Functional Theory and Strong Interactions: Orbital Ordering in Mott-Hubbard Insulators. *Phys. Rev. B* **1995**, *52*, R5467–R5470.

(10) Bo, T.; Lan, J.-H.; Zhao,Y.-L.; Zhang, Y.; He, C.-H.; Chai, Z.-F.; Shi, W-Q. First-

Principles Study of Water Adsorption and Dissociation on the UO_2 (111), (110) and (100) Surfaces. *J. Nucl. Mater*. **2014**, *454*, 446–454.

(11) Wu, X.; Ray, A. Density-Functional Study of Water Adsorption on the PuO_2 (110) Surface. *Phys. Rev. B* **2002**, *65*, 085403

(12) Jomard, G.; Bottin, F.; Geneste, G.Water Adsorption and Dissociation on the PuO_2 (110) Surface. *J. Nucl. Mater*. **2014**, *451*, 28–34.

(13) Rák, Z; Ewing, R. C.;. Becker, U. Hydroxylation-Induced Surface Stability of AnO_2 (An=U, Np, Pu) from First-Principles. *Surf. Sci*. **2013**, *608*, 180–187.

(14) Wellington, J. P. W.; Kerridge, A.; Austin, J.; Kaltsoyannis, N. Electronic Structure of Bulk AnO_2 (An = U, Np, Pu) and Water Adsorption on the (111) and (100) Surfaces of UO_2 and PuO_2 from Hybrid Density Functional Theory within the Periodic Electrostatic Embedded Cluster Method. *J. Nucl. Mat.* **2016**, *482*, 124–134.

(15) Kresse, G; Hafner, J. Ab Initio Molecular Dynamics for Liquid Metals. *Phys. Rev. B* **1993**, *47*, 558–561.

(16) Kresse, G; Hafner, J. Ab Initio Molecular-Dynamics Simulation of the Liquid-Metal–Amorphous-Semiconductor Transition in Germanium. *Phys. Rev. B* **1994**, *49*, 14251–14269.

(17) Kresse, G.; Furthmüller, J. Efficiency of Ab-Initio Total Energy Calculations for Metals and Semiconductors Using a Plane-Wave Basis Set. *Comput. Mater. Sci*. **1996**, *6*, 15–50.

(18) Kresse, G.; Furthmüller, J. Efficient Iterative Schemes for Ab Initio Total-Energy Calculations Using a Plane-Wave Basis Set. *Phys. Rev. B* **1996**, *54*, 11169–11186.

(19) Blöchl, P. E. Projector Augmented-Wave Method. *Phys. Rev. B* **1994**, *50*, 17953–17979.

(20) Kresse, G.; Joubert, D. From Ultrasoft Pseudopotentials to the Projector Augmented-Wave Method. *Phys. Rev. B* **1999**, *59*, 1758–1775.

(21) Monkhorst, H. J.; Pack, J. D. Special Points for Brillouin-Zone Integrations. *Phys. Rev. B* ***1976***, *13*, 5188–5192.

(22) Perdew, J. P.; Burke, K.; Ernzerhof, M. Generalized Gradient Approximation Made Simple [Phys. Rev. Lett. 77, 3865 (1996)]. *Phys. Rev. Lett*. **1997**, *78*, 1396–1396.

(23) Schoenes, J. Optical Properties and Electronic Structure of UO_2. *J. Appl. Phys*. **1978**, *49*, 1463–1465.

(24) McCleskey, T. M.; Bauer, E.; Jia, Q.; Burrell, A. K.; Scott, B. L.; Conradson, S.D.; Mueller, A.; Roy, L.; Wen, X.; Scuseria, G. E.; Martin. R. L. Optical Band Gap of NpO_2 and PuO_2 from Optical Absorbance of Epitaxial Films. *J. Appl. Phys*. **2013**, *113*, 013515.

(25) Molinari, M.; Parker, S. C.; Sayle, D. C.; Islam, M. S. Water Adsorption and Its Effect on the Stability of Low Index Stoichiometric and Reduced Surfaces of Ceria. *J. Phys. Chem. C* **2012**, *116*, 7073–7082.

(26) Momma, K; Izumi, F. VESTA 3 for Three-Dimensional Visualisation of Crystal, Volumetric and Morphology Data. *J. Appl. Cryst.* **2011**, *44*, 1272–1276.

(27) Bottin, F.; Geneste, G.; Jomard, G. Thermodynamic Stability of the UO_2 Surfaces: Interplay between Over-Stoichiometry and Polarity Compensation. *Phys. Rev. B* **2016**, *93*, 115438.

(28) Prodan, I. D.; Scuseria, G. E.; Martin, R. L. Assessment of Metageneralized Gradient Approximation and Screened Coulomb Hybrid Density Functionals on bulk Actinide Oxides, *Phys. Rev. B* **2006**, *73*, 045104.

(29) Alexandrov, V; Shvareva, T. Y.; Hayun, S; Asta, M; Navrotsky, A. Actinide Dioxides in Water: Interactions at the Interface. *J. Phys. Chem. Lett.* **2011**, *2*, 3130–3134.

(30) Wu, Z; Li, M; Mullins, D. R.; Overbury, S. H. Probing the Surface Sites of CeO_2

Nanocrystals with Well-Defined Surface Planes via Methanol Adsorption and Desorption. *ACS Catal*. **2012**, *2*, 2224–2234.

(31) Mullins, D. R. The Surface Chemistry of Cerium Oxide. *Surf. Sci. Rep*. **2015**, *70*, 42–85.

(32) Bo, T.; Lan, J.-H.; Zhao,Y.-L.; Zhang, Y.; He, C.-H.; Chai, Z.-F.; Shi, W-Q. Surface Properties of NpO_2 and Water Reacting with Stoichiometric and Reduced NpO_2 (111), (110), and (100) Surfaces from Ab Initio Atomistic Thermodynamics. *Surf. Sci*. **2016**, *644*, 153–164.

(33) Arrouvel, C.; Digne, M.; Breysse, M.; Toulhoat, H.; Raybaud, P. Effects of Morphology on Surface Hydroxyl Concentration: a DFT Comparison of Anatase–TiO_2 and γ-Alumina Catalytic Supports. *J. Catal*., **2004**, *222*, 152–166.

(34) Sun, Q; Reuter, K.; Scheffler, M. Effect of a Humid Environment on the Surface Structure of RuO_2(110). *Phys. Rev. B* **2003**, *67*, 205424.

(35) Kerisit, S.; Marmier, A.; Parker, S. C. Ab Initio Surface Phase Diagram of the {1014} Calcite Surface. *J. Phys. Chem. B* **2005**, *109*, 18211–18213.

(36) Data from http://kinetics.nist.gov/janaf/html/H-064.html

TOC Graphic